Pronounced Effects of Zero-Point Energy Difference on Intramolecular Electron Transfer in Asymmetric Mixed-Valence Biferrocenium Cations: Structural, EPR, and ^{57}Fe Mössbauer Characteristics

Teng-Yuan Dong*,† Ling-Shao Chang,† Gene-Hsiang Lee,‡ and Shie-Ming Peng‡

Department of Chemistry, National Sun Yat-Sen University, Kaohsiung, Taiwan, and Department of Chemistry, National Taiwan University, Taipei, Taiwan

Received April 30, 2002

The X-ray structural determinations of a series of asymmetric mixed-valence biferrocenium cations have been determined. The observations of the structural characteristics of the series of mixed-valence biferrocenium cations are also consistent with our Mössbauer studies. The features in the Mössbauer spectra of the asymmetric biferrocenium salts include two doublets, one with a quadrupole splitting of 1.5−2.2 mms^{-1} (Fe(II) site) and the other with a quadrupole splitting of 0.7−0.5 mms^{-1} (Fe(III) site). This pattern of two doublets is expected for a mixed-valence biferrocenium cation, which is valence-trapped on the time scale of the Mössbauer technique. Our data indicate that the zero-point energy difference plays a crucial role in determining the nature of the intramolecular electron-transfer rate. The electrochemical measurements and the EPR data are also described.

Introduction

The electronic interaction and the electron-transfer process between the two iron centers in the series of mixed-valence biferrocenium salts (**1**) have been extensively studied to understand what factors influence the electronic structures of the iron sites.[1−19] The first strategy is the use of a series of mixed-valence biferrocenium cations with short alkyl substituents (**1a**−**f**).[1−5] Compounds **1a**, **1e**, and **1f** give valence-localized Mössbauer spectra. At temperatures below 300 K, the spectrum shows two doublets, one for the Fe(II) metallocene and the other for the Fe(III) metallocene (electron-transfer rate < ∼10^8 s^{-1}). However, compounds **1b**−**d** show temperature-dependent Mössbauer spectra. At temperatures below 77 K, they show localized Mössbauer spectra (two doublets).

In each case the two doublets move together with increasing temperature and eventually become a single "average-valence" doublet at temperatures of 275, 260, and 275 K, respectively. The single X-ray structural determinations revealed that the environment surrounding a cation is perhaps the most important factor in determining the rate of electron transfer. Hendrickson also suggested that the temperature dependence of

Chart 1

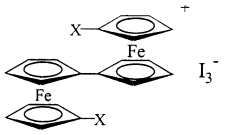

1

a. X= −CH_3 **j.** X= −$C_{10}H_{21}$
b. X= −C_2H_5 **k.** X= −$C_{12}H_{25}$
c. X= −C_3H_7 **l.** X= −$C_{13}H_{27}$
d. X= −C_4H_9 **m.** X= −$C_{15}H_{31}$
e. X= −C_5H_{11} **n.** X= −$C_{17}H_{35}$
f. X= −C_6H_{13} **o.** X= −$C_{19}H_{39}$
g. X= −C_7H_{15} **p.** X= −$(CH_2)_nC_6H_5$
h. X= −C_8H_{17} **q.** X= −napthylmethyl
i. X= −C_9H_{19}

† National Sun Yat-Sen University.
‡ National Taiwan University.

(1) Hendrickson, D. N.; Oh, S. M.; Dong, T.-Y.; Kambara, T.; Cohn, M. J.; Moore, M. F. *Comments Inorg. Chem.* **1985**, *4*, 329.
(2) Dong, T.-Y.; Hendrickson, D. N.; Iwai, K.; Cohn, M. J.; Geib, S. J.; Rheingold, A. L.; Sano, H.; Motoyama, I.; Nakashima, S. *J. Am. Chem. Soc.* **1985**, *107*, 7996.
(3) Dong, T.-Y.; Hendrickson, D. N.; Pierpont, C. G.; Moore, M. F. *J. Am. Chem. Soc.* **1986**, *108*, 963.
(4) Iijima, S.; Saida, R.; Motoyama, I.; Sano, H. *Bull. Chem. Soc. Jpn.* **1981**, *54*, 1375.
(5) (a) Nakashima, S.; Katada, M., Motoyama, I.; Sano, H. *Bull. Chem. Soc. Jpn.* **1987**, *60*, 2253. (b) Nakashima, S.; Katada, M.; Motoyama, I.; Sano, H. *Bull. Chem. Soc. Jpn.* **1986**, *59*, 2923. (c) Nakashima, S.; Masuda, Y.; Motoyama, I.; Sano, H. *Bull. Chem. Soc. Jpn.* **1987**, *60*, 1673. (d) Nakashima, S.; Oka, T.; Okuda, T.; Watanabe, M. *Inorg. Chem.* **1999**, *38*, 4005.
(6) Kai, M.; Katada, M., Sano, H. *Chem. Lett.* **1988**, 1523.
(7) Dong, T.-Y.; Schei, C. C.; Hsu, T. L.; Lee, S. L.; Li, S. J. *Inorg. Chem.* **1991**, *30*, 2457.
(8) Dong, T.-Y.; Chou, C. Y. *J. Chem. Soc., Chem. Commun.* **1990**, 1332.
(9) Dong, T.-Y.; Schei, C. C.; Hwang, M. Y.; Lee, T. Y.; Yeh, S. K.;. Wen, Y. S. *Organometallics* **1992**, *11*, 573.
(10) Webb, R. J.; Geib, S. J.; Staley, D. L.; Rheingold, A. L.; Hendrickson, D. N. *J. Am. Chem. Soc.* **1990**, *112*, 5031.
(11) Webb, R. J.; Rheingold, A. L.; Geib, S. J.; Staley, D. L.; Hendrickson, D. N. *Angew. Chem., Int. Ed. Engl.* **1989**, *28*, 1388.
(12) Dong, T.-Y.; Kambara, T.; Hendrickson, D. N. *J. Am. Chem. Soc.* **1986**, *108*, 5857.
(13) Dong, T.-Y.; Kambara, T.; Hendrickson, D. N. *J. Am. Chem. Soc.* **1986**, *108*, 4423.
(14) Gang, H. G.; S. Geib, J.; Kaneko, Y.; Nakano, M.; Sorai, M.; Rheingold, A. L.; Montez, B.; Hendrickson, D. N. *J. Am. Chem. Soc.* **1989**, *111*, 173.
(15) Kaneko, Y.; Nakano, M.; Sorai, M.; Jang, H. G.; Hendrickson, D. N. *J. Am. Chem. Soc.* **1989**, *28*, 1067.
(16) Dong, T.-Y.; Lee, T. Y.; Lin, M. H. *J. Organomet. Chem.* **1992**, *427*, 101.
(17) Dong, T.-Y.; Chang, C. K.; Huang, C. H.; Wen, Y. S.; Lee, S. L.; Chen, J. A.; Yeh, W. Y.; Yeh, A. *J. Chem. Soc., Chem. Commun.* **1992**, 526.
(18) Dong, T.-Y.; Huang, C. H.; Chang, C. K.; Wen, Y. S.; Lee, S. L.; Chen, J. A.; Yeh, W. Y.; Yeh, A. *J. Am. Chem. Soc.* **1993**, *115*, 6357.
(19) Dong, T.-Y.; Lee, S. H.; Chang, C. K.; Lin, H. M.; Lin, K. J. *Organometallics* **1997**, *16*, 2773.

10.1021/om0203476 CCC: $22.00
Publication on Web 08/29/2002

the Mössbauer spectrum is due to the onset of lattice dynamics associated with the triiodide anion and alkyl substituents.[1−3] The second strategy is the use of the mixed-valence biferrocenium salts with long alkyl substituents (**1g**−**o**).[20,21] It has been shown that there is an even−odd character in the number of carbon atoms of the substituents in the relationship between the crystal structure and the mixed-valence state. However, there is a problem in this even−odd character. That is, only the compounds with an 8- and 10-carbon alkyl substituent give a temperature-dependent detrapped-valence state. Therefore, it seems difficult to separate the contribution of the symmetry of the cation and the packing effect in the crystal. The third strategy is the use of the derivatives attached to a planar substituent (**1p**−**q**).[22−24] The 2-phenylethyl and 4-phenylbutyl derivatives of **1p** show the valence detrapping electronic state at temperatures of 300 and 160 K, respectively. By comparison of the Mössbauer results of **1p** with those of the corresponding dialkyl derivatives, the terminal benzene ring in **1p** plays an important role in controlling the rate of electron transfer. A recent interesting finding is that the mixed-valence compound **1q** has two distinct crystallographic phases that show the electron-transfer rates are extremely sensitive to changes in the crystal lattice.[22,23] The crystal in the space group $P\bar{1}$ shows a Mössbauer spectrum characteristic of a valence-detrapped electronic state above 130 K. The crystal in the space group $P2_1/n$ shows a valence-trapped Mössbauer spectrum at 300 K. In **1p** and **1q**, there is a close connection between the mixed-valence state and the cation−cation interaction formed through the $\pi-\pi$ interaction of the benzene rings.

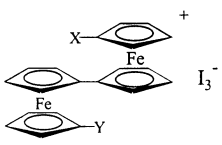

a. X= $-C_5H_{11}$ Y= −H
b. X= $-C_5H_{10}Br$ Y= −H
c. X= $-C_5H_{11}$ Y= $-C_5H_{10}Br$
d. X= $-C_5H_{10}Br$ Y= $-C_5H_{10}Br$
e. X= $-C_6H_{12}Br$ Y= $-C_6H_{12}Br$

2

Our strategy for systematic design is to use derivatives (**2a**−**e**) with terminal bromide in the alkyl substituents. If the symmetry of the cation and the intermolecular interactions (cation−cation and cation−anion interactions) are indeed important to the mixed-valence state, the terminal bromide in the alkyl substituent would then play an important role. The results of the X-ray structural determinations with the electrochemical measurements, variable-temperature Mössbauer data, and EPR measurements are presented in this paper.

Results and Discussion

Synthesis and Characterization. The biferrocenyl derivatives described in this paper were all prepared by a similar approach (Scheme 1). The sample of biferrocene was treated with acyl chloride and $AlCl_3$ and was converted into acylbiferrocene (**3a**−**e**). Reduction was carried out by stirring a mixture of corresponding acylbiferrocene with $LiAlH_4/AlCl_3$ or with Zn/Hg at ambient temperature under N_2. The neutral substituted biferrocenes **4a**−**e** were characterized by mass and ^1H NMR spectroscopies.

Molecular Structures of 1e, 2b, 2c, 2d, and 2e. X-ray crystallographic studies were undertaken to help elucidate the structures and the assignment of the oxidation state for a given ferrocenyl moiety. Figures 1−5 display the ORTEP drawing of the mixed-valence compounds **1e** and **2b**−**e**. They adopt the usual trans conformation as found for most biferrocenium cations.[1−19] Details of the X-ray crystal data collections and unit cell parameters are given in Table 1. Selected bond distances and angles are given in Tables 2 and 3, and complete tables of positional parameters, bond distances, and bond angles are given as Supporting Information. A comparison of **1e**, **2b**, **2c**, **2d**, and **2e** with the series of biferrocenium salts was also made (Table 4).

In compounds **1e**, **2b**, **2c**, and **2e**, the two metallocene moieties in each cation are not crystallographically equivalent. In the case of **2d**, the refinement of the structure imposed inversion centers on both the cation and the triiodide anion. Therefore, the two ferrocenyl moieties are crystallographically equivalent. It has been demonstrated that the iron to the Cp ligand bond length and the Fe−C bond distance give a diagnosis of the oxidation state of the iron center. In a localized biferrocenium cation, the Fe−Cp and Fe−C distances for an Fe(II) center are closer to the corresponding values of 1.65 and 2.045 Å found[25] for ferrocene, and the Fe−Cp and Fe−C distances for an Fe(III) center are closer to the corresponding values of 1.70 and 2.075 Å found[26] for ferrocenium ion. However, in a delocalized biferrocenium cation, both Fe−Cp and Fe−C distances are intermediate between the analogous values for ferrocene and ferrocenium ion. As shown in Table 4, the oxidation state of the Fe center in each ferrocenyl moiety of **1e**, **2b**, **2c**, and **2e** is assigned on the basis of the Fe−Cp and Fe−C distances. This indicates that the valence state of **1e**, **2b**, **2c**, and **2e** is in a trapped-valence state. In the case of **2d**, the mean Fe−C distance is 2.060(5) Å, between the values of 2.045 Å for ferrocene[25] and 2.075 Å for ferrocenium cation,[26] indicating that the valence state is in a detrapped-valence state at room temperature. This result is in accordance with the result of ^{57}Fe Mössbauer spectra. Furthermore, the dihedral angle between the two least-squares planes and the average staggering angle of the two Cp rings in each ferrocenyl moiety are also collected in Table 4. Furthermore, in the case of mixed-valence cation **2b**, the bromopentyl substituent is found to be rotationally disordered, with two sites in the population ratio of 80:20.

As shown in Table 2, the triiodide anion in **1e**, **2b**, **2c**, and **2e** shows an asymmetric structure. In the case of **2d**, the triiodide anion is at the inversion center, showing a symmetric structure. The I−I distance in **2d** is 2.916(1) Å.

(20) Nakashima, S.; Nakszaki, S.; Sakai, H.; Watanabe, M.; Motoyama, I.; Sato, M. *Inorg. Chem.* **1998**, *37*, 1959.
(21) Nakashima, S.; Ueki, Y.; Sakai, H. *J. Chem. Soc., Dalton Trans.* **1995**, 513.
(22) (a) Dong, T.-Y.; Lai, X. Q.; Lin, Z. W.; Lin, K. J. *Angew. Chem., Int. Ed. Engl.* **1997**, *36*, 2002. (b) Nakashima, S.; Hori, A.; Sakai, H.; Watanabe, M.; Motoyama, I. *J. Organomat. Chem.* **1997**, *542*, 271.
(23) Dong, T.-Y.; Ho, P. H.; Lai, X. Q.; Lin, Z. W.; Lin, K. J. *Organometallics* **2000**, *19*, 1096.
(24) Webb, R. J.; Dong, T.-Y.; Pierpont, C. G.; Boone, S. R.; Chadha, R. K.; Hendrickson, D. N. *J. Am. Chem. Soc.* **1991**, *113*, 4806.
(25) Seiler, P.; Dunitz, J. D. *Acta Crystallogr. B* **1979**, *35*, 1068.
(26) Mammano, N. J.; Zalkin, A.; Landers, A.; Rheingold, A. L. *Inorg. Chem.* **1977**, *16*, 297.

Scheme 1

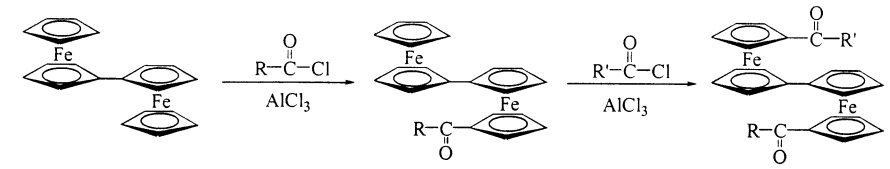

3a R= $-C_4H_9$
b R= $-C_4H_8Br$

3c R= $-C_4H_9$ R'= $-C_4H_8Br$
d R=R'= $-C_4H_8Br$
e R=R'= $-C_5H_{10}Br$

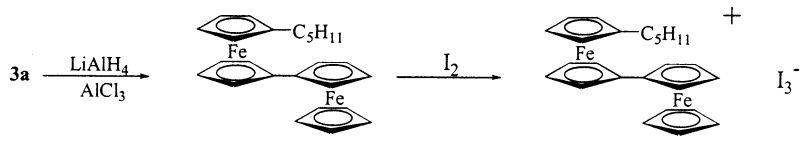

4a **2a**

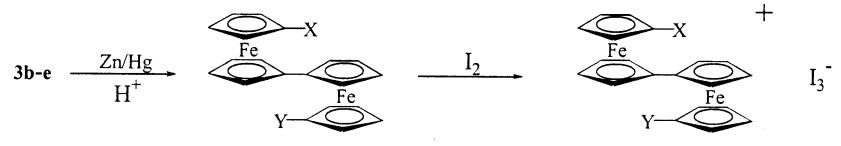

2b-e

4b X= $-C_5H_{10}Br$ Y= $-H$
4c X= $-C_5H_{11}$ Y= $-C_5H_{10}Br$
4d X=Y= $-C_5H_{10}Br$
4e X=Y= $-C_6H_{12}Br$

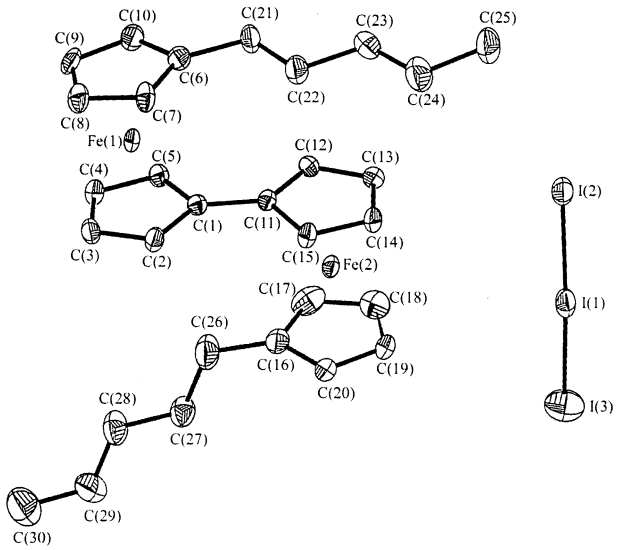

Figure 1. ORTEP drawing for **1e** at 150 K.

Cyclic Voltammetric Studies. One of the interesting attributes of **2a**−**e** is the magnitude of the interaction between the two Fe sites. Cyclic voltammetry affords a simple and effective way for estimating this interaction.[27] Electrochemical data of the neutral compounds **4a**−**e** are shown in Table 5. The CV studies of **4a**−**e** show two successive one-electron oxidations that correspond to the oxidation of the biferrocenyl moiety. As shown in Table 5, the first half-wave potential of 1′,1‴-dipentylbiferrocene (−0.06 V) is less than those of **4a** and **4b** (−0.03 and −0.02 V, respectively). From the electron-donating effect of the alkyl substituent, we believe that the first oxidation in **4a** and **4b** occurs at the alkylferrocenyl moiety. This is also consistent with our X-ray structural study of **2b**. In the case of **4c**, it is difficult to predict which ferrocenyl moiety is oxidized first from the electrochemical data.

It has been demonstrated that the magnitude of the peak-to-peak separation ($\Delta E_{1/2}$) gives an indication of the interaction between the two Fe sites.[27] A comparison of the magnitude of $\Delta E_{1/2}$ between 1′,1‴-dipentylbiferrocene and **4c** indicates that the magnitudes of interactions between the two Fe sites in symmetric and asymmetric biferrocenium cations are similar in the solution state. This indicates that the interactions between the two Fe sites are insensitive to the nature of the substituent. Thus, the zero-point energy difference between the two vibronic states for each asymmetric biferrocenium cation is rather small, which is reasonable in terms of the similar electronic effect between

(27) (a) Atzkern, H.; Huber, B.; Köhler, F. H.; Müller, G.; Müller, R. *Organometallics* **1991**, *10*, 238. (b) Bunel, E. E.; Campos, P.; Ruz, P.; Valle, L.; Chadwick, I.; Ana, M. S.; Gonzalez, G.; Manriquez, J. M. *Organometallics* **1988**, *7*, 474. (c) Cowan, D. O.; Shu, P.; Hedberg, F. L.; Rossi, M.; Kistenmacher, T. J. *J. Am. Chem. Soc.* **1979**, *101*, 1304. (d) Moulton, R.; Weidman, T. W.; Vollhardt, K. P. C.; Bard, A. J. *Inorg. Chem.* **1986**, *25*, 1846. (e) Obendorf, D.; Schottenberger, H.; Rieker, C. *Organometallics* **1991**, *10*, 1293.

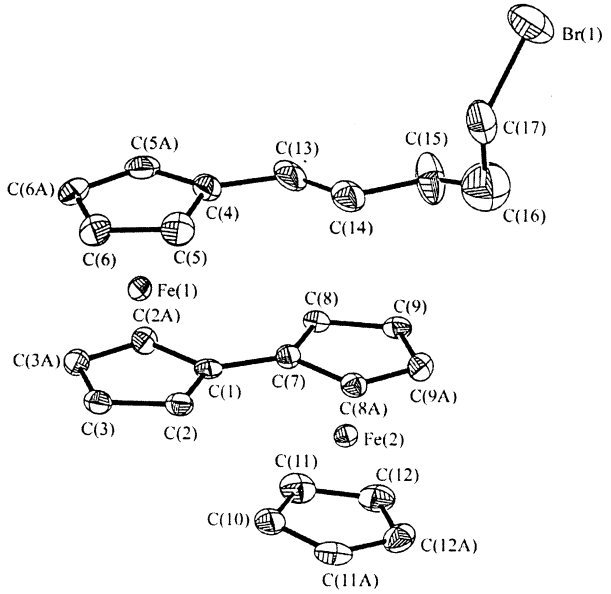

Figure 2. ORTEP drawing for **2b** at 150 K.

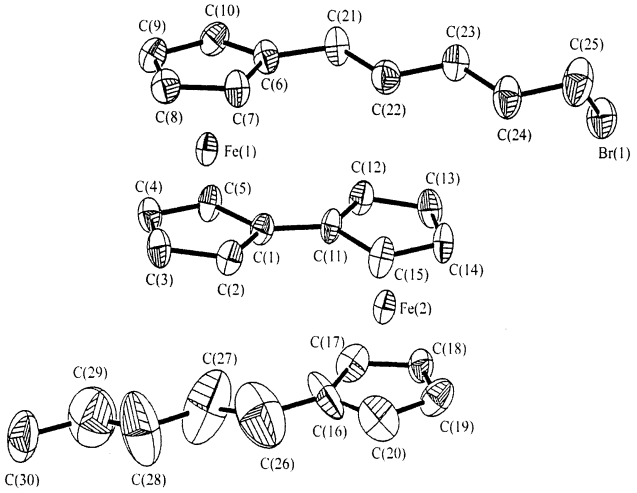

Figure 3. ORTEP drawing for **2c** at 295 K.

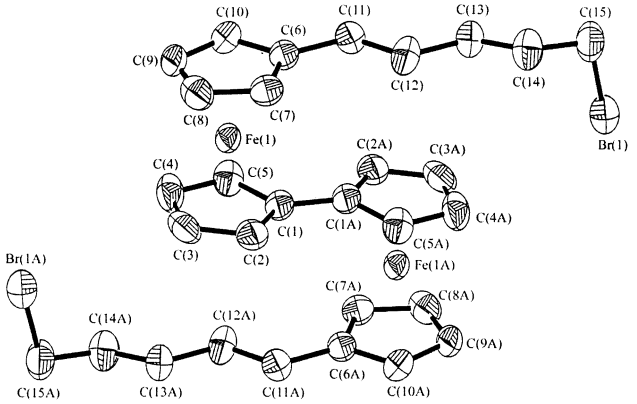

Figure 4. ORTEP drawing for **2d** at 295 K.

the pentyl substituent and the bromopentyl substituent on the biferrocenium cation in the solution state.

^{57}Fe Mössbauer Characteristics. It has been noted that the ^{57}Fe Mössbauer spectral properties of 1′,1‴-dialkylbiferrocenium triiodide cations are dependent on the sample history.[2,3] To examine this phenomenon more thoroughly, we prepared samples of **1e** and **2a**−**e** by two different methods. Microcrystalline samples were prepared by adding a benzene/hexane (1:1) solution containing a stoichiometric amount of iodine to a benzene/hexane (1:1) solution of the corresponding neutral biferrocene at 0 °C. A crystalline sample can be prepared by slowly diffusing hexane into a CH_2Cl_2 solution containing the corresponding biferrocenium triiodide salt.

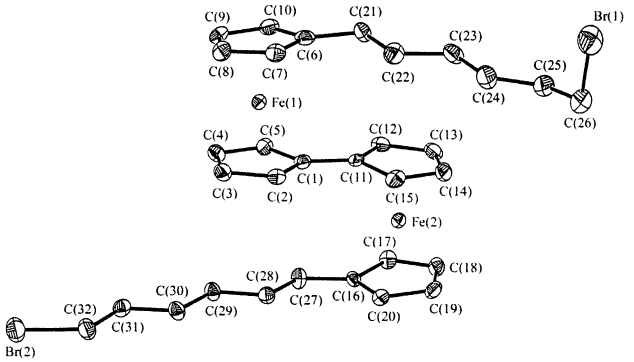

Figure 5. ORTEP drawing for **2e** at 150 K.

Mössbauer spectra were run for microcrystalline and crystalline samples of **1e** and **2a**−**e**. The various absorption peaks in each spectrum were fitted to Lorentzian lines, and the resulting fitting data are summarized in Table 6. The selected variable-temperature Mössbauer spectra are also shown in Figures 6−8.

The features in all 300 and 80 K Mössbauer spectra of asymmetric microcrystalline biferrocenium salts **2a**, **2b**, and **2c** include two doublets, one with a quadrupole splitting (ΔE_Q) of 1.5−2.2 mm s^{-1} (Fe(II) site) and the other with a ΔE_Q of 0.7−0.5 mm s^{-1} (Fe(III) site). This pattern of two doublets is expected for a mixed-valence biferrocenium cation that is valence-trapped on the time scale of the Mössbauer technique (electron-transfer rate $< \sim 10^7$ s^{-1} in the solid state). In the cases of microcrystalline and crystalline samples of symmetric biferrocenium salts (**1e**, **2c**, and **2e**), two doublets can be seen at 300 and 80 K Mössbauer spectra, one characteristic of an Fe(II) metallocene and the other characteristic of an Fe(III) metallocene. As a typical example, the 300 and 80 K Mössbauer spectra of **2c** are shown in Figure 6. However, it was curious to find that the two different preparations of symmetric biferrocenium salt **2d** showed temperature-dependent Mössbauer spectra. Figures 7 and 8 illustrate the spectra obtained for the samples prepared by two different preparations. At 80 K, the two samples show two doublets in the Mössbauer spectra. An increase of temperature causes the two doublets to move together, resulting in an average-valence doublet at 150 and 120 K for both microcrystalline and crystalline samples, respectively.

In the case of localized mixed-valence biferrocenium salts **1e**, **2a**, **2b**, **2c**, and **2e**, the decrease of ΔE_Q in the ferrocenyl doublet and the increase of ΔE_Q in the ferrocenium doublet can be an indication of the magnitude of intramolecular electron-transfer rate in the mixed-valence cation. In the 300 K Mössbauer spectrum of **2c**, the value of ΔE_Q (1.551 mm s^{-1}) for the ferrocenyl moiety is smaller than what is expected for an Fe(II) ferrocenyl moiety, and the Fe(III) ferrocenium moiety has a relatively large ΔE_Q value (0.753 mm s^{-1}). This is a reflection of the mixing of Fe(II) and Fe(III) moieties

Table 1. Experimental and Crystal Data for the X-ray Structures

	1e	2b	2c	2d	2e
formula	$C_{30}H_{38}Fe_2I_3$	$C_{25}H_{27}BrFe_2I_3$	$C_{30}H_{37}BrFe_2I_3$	$C_{30}H_{36}Br_2Fe_2I_3$	$C_{32}H_{40}Br_2Fe_2I_3$
MW	891.00	899.78	969.91	1048.81	1076.86
T, K	150(1)	150(1)	295(2)	295(2)	150(1)
cryst syst	monoclinic	orthorhombic	triclinic	triclinic	triclinic
space group	$P2_1/c$	*Pnma*	$P\bar{1}$	$P\bar{1}$	$P\bar{1}$
a, Å	23.5809(3)	20.6427(5)	9.720(3)	9.512(2)	9.8734(1)
b, Å	9.4328(1)	9.5825(2)	11.512(3)	9.882(2)	10.4073(1)
c, Å	14.0037(1)	13.5032(3)	15.030(4)	10.829(2)	18.4792(3)
α, deg	90	90	104.48(3)	110.05(2)	80.924(1)
β, deg	96.913(1)	90	97.98(3)	114.22(2)	77.663(1)
γ, deg	90	90	91.32(3)	98.98(2)	67.498(1)
V, A^3	3092.25(6)	2671.0(1)	1609.7(8)	818.0(3)	1707.68(4)
Z	4	4	2	1	2
D_{calcd}, gcm^{-3}	1.914	2.237	2.001	2.129	2.094
μ, mm^{-1}	3.950	6.061	5.037	6.178	5.922
F(000)	1716	1692	926	497	1026
λ, Å	0.71073	0.71073	0.71073	0.71073	0.71073
θ limits, deg	27.50	27.50	24.97	27.50	27.50
R_1	0.0437	0.0531	0.0573	0.0377	0.0446
wR_2	0.0823	0.1218	0.1551	0.0927	0.1111

Table 2. Selected Bond Distances and Angles of 1e, 2c, 2d, and 2e

	1e	2c	2d	2e
I1−I2	2.8721(5)	2.913(1)	2.916(1)	2.9305(5)
I1−I3	2.9853(5)			
I3−I4		2.918(2)		2.9234(4)
Fe1−C1	2.043(4)	2.065(9)	2.076(5)	2.060(5)
Fe1−C2	2.050(5)	2.062(9)	2.052(6)	2.050(5)
Fe1−C3	2.060(5)	2.04(1)	2.043(6)	2.059(6)
Fe1−C4	2.056(5)	2.05(1)	2.052(6)	2.050(6)
Fe1−C5	2.045(5)	2.05(1)	2.054(5)	2.047(6)
Fe1−C6	2.093(5)	2.05(1)	2.107(5)	2.083(6)
Fe1−C7	2.059(5)	2.04(1)	2.063(5)	2.062(6)
Fe1−C8	2.037(5)	2.04(1)	2.037(5)	2.045(6)
Fe1−C9	2.051(5)	2.06(1)	2.044(5)	2.041(6)
Fe1−C10	2.066(5)	2.10(1)	2.074(6)	2.058(6)
Fe2−C11	2.135(4)	2.122(9)		2.152(5)
Fe2−C12	2.088(5)	2.08(1)		2.088(6)
Fe2−C13	2.070(5)	2.07(1)		2.048(6)
Fe2−C14	2.076(5)	2.05(1)		2.064(6)
Fe2−C15	2.089(5)	2.08(1)		2.098(5)
Fe2−C16	2.114(5)	2.08(2)		2.146(5)
Fe2−C17	2.060(5)	2.03(1)		2.103(6)
Fe2−C18	2.048(5)	2.03(1)		2.078(5)
Fe2−C19	2.069(5)	2.08(1)		2.056(6)
Fe2−C20	2.108(5)	2.10(1)		2.091(6)
C1−C2	1.429(5)	1.45(1)	1.418(8)	1.444(8)
C1−C5	1.435(6)	1.44(1)	1.434(8)	1.443(8)
C2−C3	1.431(6)	1.39(1)	1.421(8)	1.432(8)
C3−C4	1.421(6)	1.40(1)	1.41(1)	1.433(9)
C4−C5	1.422(6)	1.44(1)	1.425(8)	1.433(8)
C6−C7	1.425(6)	1.41(1)	1.411(8)	1.431(8)
C6−C10	1.420(6)	1.40(1)	1.414(8)	1.419(9)
C7−C8	1.417(7)	1.40(1)	1.434(8)	1.426(9)
C8−C9	1.406(7)	1.43(1)	1.384(9)	1.430(9)
C9−C10	1.416(6)	1.43(1)	1.412(8)	1.434(8)
C11−C12	1.437(5)	1.42(1)		1.430(8)
C11−C15	1.438(6)	1.42(1)		1.436(8)
C12−C13	1.421(6)	1.44(1)		1.429(9)
C13−C14	1.421(6)	1.40(1)		1.41(1)
C14−C15	1.422(6)	1.42(1)		1.430(8)
C16−C17	1.410(7)	1.38(2)		1.425(7)
C16−C20	1.416(7)	1.39(2)		1.426(8)
C17−C18	1.437(8)	1.36(2)		1.416(8)
C18−C19	1.413(8)	1.41(2)		1.418(9)
C19−C20	1.403(7)	1.40(2)		1.436(8)
I2−I1−I2		180.00(3)	180.0	180.0
I2−I1−I3	178.53(2)			
I4−I3−I4		180.00(3)		180.0

Table 3. Selected Bond Distances and Angles of 2b

I1−I2	2.998(1)	I1−I3	2.920(1)
Fe1−C1	2.16(1)	Fe1−C2	2.100(7)
Fe1−C3	2.066(7)	Fe1−C4	2.16(1)
Fe1−C5	2.100(8)	Fe1−C6	2.072(8)
Fe2−C7	2.04(1)	Fe2−C8	2.050(7)
Fe2−C9	2.065(7)	Fe2−C10	2.03(1)
Fe2−C11	2.055(8)	Fe2−C12	2.065(8)
C1−C2	1.43(1)	C2−C3	1.42(1)
C3−C3[a]	1.44(2)	C4−C5	1.44(1)
C5−C6	1.42(1)	C6−C6[a]	1.44(2)
C7−C8	1.449(9)	C8−C9	1.42(1)
C9−C9[a]	1.44(2)	C10−C11	1.43(1)
C11−C12	1.41(1)	C12−C12[a]	1.42(2)
I3−I1−I2	177.57(4)		

[a] Symmetry transformation used to generate equivalent atom: *x*, $-y + 1/2$, *z*.

into the ground state. At 300 K, the respective values of $\Delta\Delta E_Q$, which is the difference of ΔE_Q between Fe(II) and Fe(III) moieties, for **1e**, **2a**, **2b**, **2c**, and **2e** are 1.346, 1.833, 1.814, 0.798, and 1.454 mm s^{-1}. Thus, the order of the intramolecular electron-transfer rate appears to be **2c** > **1e** ≈ **2e** > **2b** ≈ **2a**. In general, the factors that are potentially important in controlling the intramolecular electron-transfer rate in a mixed-valence biferrocenium cation include (1) the electronic coupling between the two Fe centers and the vibronic coupling, which is a measure of the difference in bond lengths of the ferrocenyl moieties in the two different Fe(II) and Fe(III) oxidation states, (2) the zero-point energy difference between the two vibronic states, and (3) the intermolecular cation−cation and cation−anion interactions. The evidence of the studies of electrochemical measurements and single-crystal X-ray structural determinations indicates that the electronic and vibronic couplings in the series of mixed-valence biferrocenium salts are similar. The ligand field strength around the Fe center is similar. A change in valence in a mixed-valence biferrocenium cation is accompanied by a sizable coordination sphere reorganization. In the series of mixed-valence biferrocenium cations, the change of the distance between the Fe center and the Cp ring centroid from the Fe(II) ferrocenyl moiety (1.65 Å) to the Fe(III) ferrocenium moiety (1.70 Å) is also similar. Therefore, we believe that the difference in electron-transfer rates in **1e** and **2a**−**e** is the result of the magnitude of the zero-point energy difference and the intermolecular interactions.

We believe that the most important factor in controlling the intramolecular electron-transfer rate is the

Table 4. Comparison of the Atomic Distances

compd	T (K)[a]	Fe−C	Fe−Cp[b]	tilt angle[c]	stagger angle[d]	T_c (K)[e]	site
1b	300	2.06(1)	1.676(5)	4.8		275	
1c	300	2.06(1)	1.677(9)	6.6	1.2	245	
1e[f,k]	150(1)	2.056(5)	1.663	2.80	9.4	loc.[g]	Fe(II)
		2.086(5)	1.700	2.39	9.2		Fe(III)
1g[f]	300	2.08(2)	1.69	4.17		loc.[g]	Fe(III)
		2.06(1)	1.66	2.97			Fe(II)
1h[f,h]	300	2.06(2)		2.43		∼210	
		2.06(2)		4.67			
		2.05(2)		4.06			
		2.05(2)		4.23			
1k	300	2.067				∼230	
1q	300[i]	2.059(5)	1.672(2)	4.4	7.0	115	
	300[j]	2.052(4)	1.660(4)	2.1	3.0	loc.[g]	Fe(II)
		2.086(5)	1.693(4)	5.5	2.3		Fe(III)
2b[k]	150	2.100(8)	1.712	4.65	∼0	loc.[g]	Fe(III)
		2.054(8)	1.656	3.04	∼0		Fe(II)
2c[k]	295	2.06(1)	1.663	5.05	2.0	loc.[g]	Fe(II)
		2.07(1)	1.693	12.08	2.7		Fe(III)
2d[k]	295	2.060(5)	1.672	5.19	9.0	∼115	
2e[k]	150	2.056(6)	1.656	4.35	3.9	loc.[g]	Fe(II)
		2.092(6)	1.706	7.70	14.1		Fe(III)

[a] Temperature for the single-crystal X-ray structural determination. [b] Average distance of the Fe to the least-squares planes of the Cp rings. [c] Dihedral angle between the two least-squares planes of the Cp rings. [d] Average staggering angle of the two Cp rings in each ferrocenyl moiety. [e] Temperature for the localization−delocalization transition on the Mössbauer technique. [f] The two ferrocenyl moieties are not crystallographically equivalent. The data associated with Fe1 are listed first. [g] The electron-transfer rate is localized on the Mössbauer time scale. [h] There are two independent molecules. [i] Compound **1q** exhibits two crystalline morphologies at room temperature. The crystals in $P\bar{1}$ phase were formed from CH_2Cl_2 solution. [j] Crystals in the $P2_1/n$ phase. [k] This work.

Table 5. Electrochemical Data of 4a−e

compound	$E_{1/2}$,[a] V	$\Delta E_{1/2}$,[b] V	ΔE_p,[c] mV
dipentylbifc[d]	−0.06	0.39	86
	0.34		80
4a	−0.03	0.39	108
	0.36		98
4b	−0.02	0.38	112
	0.36		104
4c	−0.05	0.39	99
	0.34		85
4d	−0.04	0.38	101
	0.34		93

[a] All half-wave potentials are referred to the nonaqueous Ag/AgCl electrode (CH_3CN as solvent). Ferrocene shows a reversible one-electron oxidation wave at $E_{1/2} = 0.12$ V in 1:1 CH_3CN and CH_2Cl_2 solution. [b] Peak separation between two redox waves. [c] Peak to peak separation between the resolved reduction and oxidation wave maxima. [d] The electrochemical data of 1′,1‴-dipentylbiferrocene.

symmetry of the cation. For an asymmetric biferrocenium cation, the two irons are not in equivalent environments and this asymmetry results in a zero-point energy difference for intramolecular electron transfer. In other words, one vibronic state[28] of the mixed-valence cation is energetically more stable than the other state. This explains why a delocalized state for an asymmetric biferrocenium cation has not been observed. Thus, the presence of a zero-point energy difference elucidates the order of the electron-transfer rate: **1e** ≈ **2e** > **2b** ≈ **2a**. However, an interesting finding is that the electron-transfer rate in the asymmetric biferrocenium cation **2c** is greater than that in the biferrocenium cation **2e**. In the solid-state structure

(28) Wong, K. Y.; Schatz, P. N. *Prog. Inorg. Chem.* **1981**, *28*, 369.

Table 6. ^{57}Fe Mössbauer Least-Squares-Fitting Parameters

compound	T, K	ΔE_Q[a]	δ[b]	Γ[c]
1e[d]	300	1.880	0.460	0.389, 0.389
		0.534	0.408	0.256, 0.256
		2.025	0.539	0.234, 0.237
		0.526	0.529	0.356, 0.331
2a[d]	300	2.180	0.437	0.258, 0.290
		0.347	0.432	0.357, 0.386
	80	2.167	0.525	0.273, 0.261
		0.372	0.531	0.327, 0.360
2b[d]	300	2.199	0.449	0.277, 0.272
		0.385	0.434	0.299, 0.276
	80	2.152	0.522	0.266, 0.277
		0.458	0.516	0.326, 0.378
2c[d]	300	1.551	0.461	0.416, 0.416
		0.753	0.410	0.383, 0.383
	80	1.807	0.534	0.391, 0.391
		0.777	0.536	0.424, 0.424
2c[e]	300	1.589	0.461	0.422, 0.422
		0.749	0.419	0.395, 0.395
	80	1.792	0.528	0.403, 0.372
		0.781	0.536	0.437, 0.402
2d[d]	300	1.187	0.439	0.384, 0.414
	150	1.232	0.515	0.558, 0.553
	140	1.481	0.510	0.458, 0.459
		1.005	0.524	0.448, 0.434
	120	1.500	0.528	0.450, 0.486
		1.015	0.523	0.443, 0.439
	90	1.585	0.534	0.452, 0.472
		0.960	0.536	0.441, 0.458
	80	1.605	0.532	0.465, 0.470
		0.933	0.550	0.451, 0.431
2d[e]	300	1.135	0.442	0.380, 0.398
	150	1.180	0.502	0.440, 0.454
	140	1.191	0.505	0.447, 0.468
	130	1.200	0.511	0.473, 0.465
	120	1.196	0.509	0.477, 0.481
	110	1.454	0.521	0.392, 0.385
		0.967	0.514	0.363, 0.365
	100	1.479	0.519	0.385, 0.383
		0.956	0.519	0.350, 0.382
	90	1.524	0.527	0.385, 0.393
		0.941	0.521	0.360, 0.363
	80	1.558	0.520	0.386, 0.394
		0.898	0.521	0.377, 0.356
2e[d]	300	1.946	0.424	0.344, 0.348
		0.492	0.409	0.325, 0.284

[a] Quadrupole splitting (in mm s^{-1}). [b] Isomer shift (in mm s^{-1}). [c] Full width (in mm s^{-1}) at half-height taken from the least-squares-fitting program. The width for the line at more positive velocity is listed first for the doublet. [d] Microcrystalline sample. [e] Crystalline sample.

of **2e**, the two metallocene moieties in each cation are not crystallographically equivalent and the two bromohexyl substituents on the Cp rings are situated differently. As shown in Figure 9, this asymmetry is caused mainly by the intermolecular interactions. The closest contact between cation and cation is Br1−Br2 (3.495 Å). There is also a cation−anion interaction between terminal Br and I_3^- anions (Br1···I2 = 3.997 Å and Br2···I4 = 3.904 Å). We believe that these cation−cation and cation−anion interactions in **2e** play an important role in inducing the asymmetry between the two ferrocenyl moieties in **2e**.

Electron Paramagnetic Resonance. X-band EPR spectra were run at 77 K for **1e** and **2a**−**e**. An axial-type spectrum was observed for the series of compounds. Samples that were prepared by two different preparations for a given cation gave essentially identical spectra. The g values evaluated from all of these spectra are collected in Table 7.

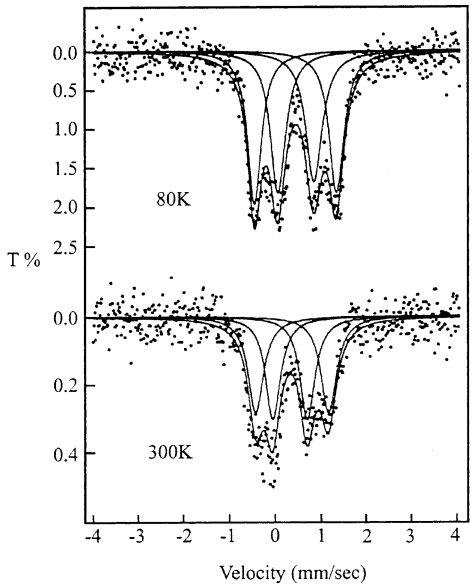

Figure 6. Variable-temperature Mössbauer spectra of a crystalline sample of **2c**.

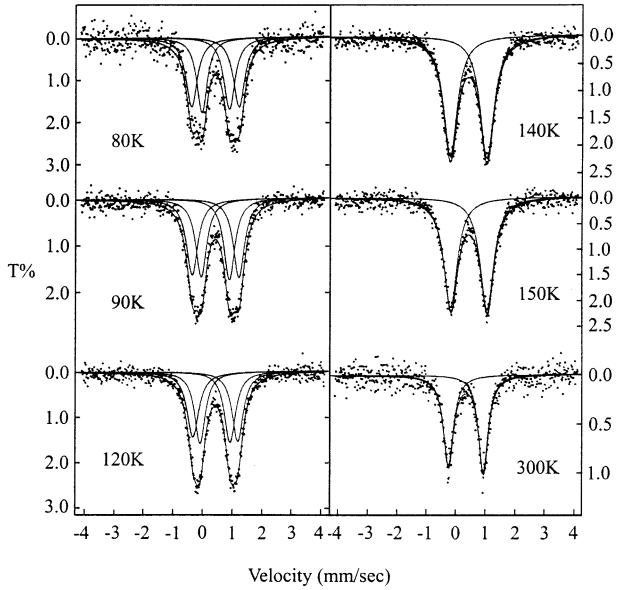

Figure 7. Variable-temperature Mössbauer spectra of a microcrystalline sample of **2d**.

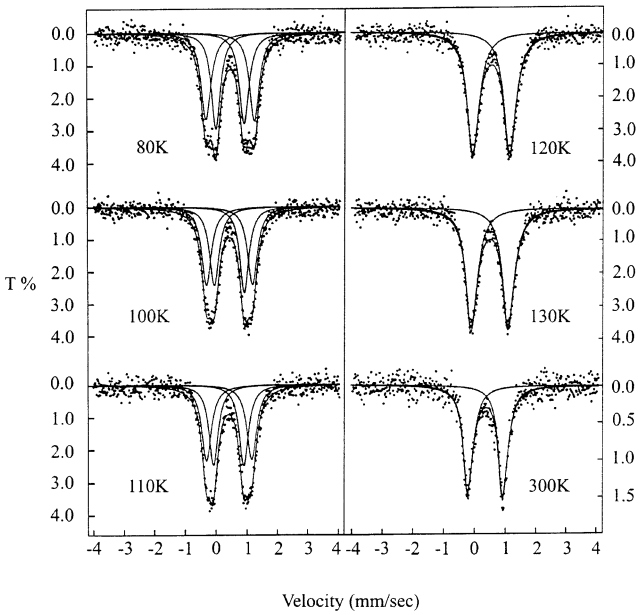

Figure 8. Variable-temperature Mössbauer spectra of a crystalline sample of **2d**.

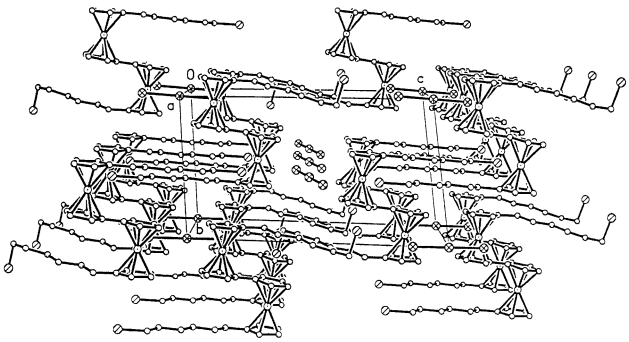

Figure 9. Packing arrangement of **2e**.

Table 7. Electron Paramagnetic Resonance Data at 77 K

compound[a]	$g_{\parallel}$	$g_{\perp}$	Δg
1e	3.30	1.87	1.42
2a	3.40	1.86	1.54
2b	3.36	1.85	1.50
2c	3.00	1.95	1.05
2d	2.97	1.96	1.01
2e	3.21	1.90	1.31

[a] Powder sample. [b] $\Delta g = g_{\parallel} - g_{\perp}$.

In a biferrocenium cation, the value of the g tensor anisotropy ($\Delta g = g_{\parallel} - g_{\perp}$) is considerably reduced, and this is a reflection of a reduced orbital angular momentum in the ground state that results from admixture of Fe(II) electronic configuration into the Fe(III) electronic configuration. In general, if the Δg value for a given mixed-valence biferrocenium cation is smaller than 0.75, then the rate of electron transfer is greater than the EPR time scale ($\sim 10^{10}$ s^{-1}).[24] From Table 7, the Δg values of **1e** and **2a**−**e** suggest that the cations in these compounds are localized on the EPR time scale at 77 K. Hence, it is consistent with the Mössbauer data. As shown in Figure 10, it appears that there is a correlation between the values of Δg and $\Delta\Delta E_Q$ (the difference of quadrupole splitting between the Fe(II) site and the Fe(III) site). Thus, the value of Δg gives an indication of the magnitude of electron-transfer rate.

Concluding Comments. In this paper, we demonstrate that the relatively minor perturbations caused by the substituents have pronounced effects on the electron structure and the rate of electron transfer. Our data indicate that the zero-point energy difference plays a crucial role in determining the nature of the intramolecular electron-transfer rate in biferrocenium cation. The terminal Br in the alkyl substituent on the Cp ring in biferrocenium cation modifies the packing arrangement of biferrocenium cation in the solid state. Furthermore, our results are different from the observation found by Nakashima.[20,21] Nakashima reported an even−odd character in the number of carbon atoms of substituents in the relationship between the crystal structure and the mixed-valence state. Compounds with a 6-, 8-, 10-, 12-, 14-, and 16-carbon alkyl substituent give a temperature-dependent detrapped-valence state. In our results, the dibromopentylbiferrocenium triiodide has a detrapped-valence state and the dibro-

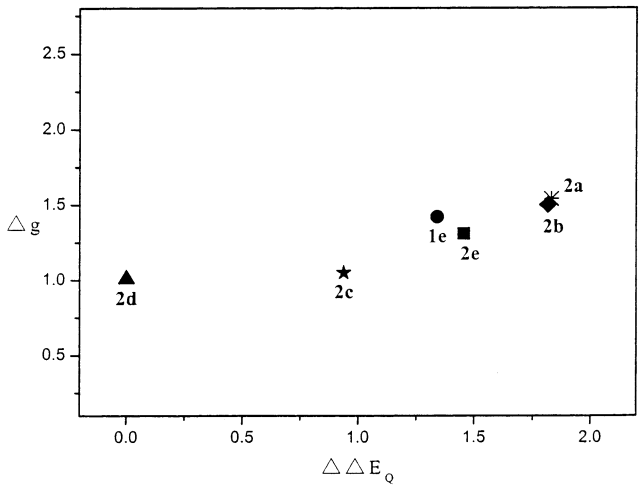

Figure 10. Correlation between Δg and $\Delta\Delta E_Q$.

mohexylbiferrocenium triiodide has a trapped-valence state.

Experiment Section

General Information. All manipulations involving air-sensitive materials were carried out by standard Schlenk techniques under an atmosphere of N_2. Chromatography was performed on neutral alumina (Merck, act. II). The sample of biferrocene was prepared according to the literature procedure.[29]

Acylation of Biferrocene. The acylating reagent was made up according to the Friedel−Crafts synthesis by mixing acyl chloride and excess $AlCl_3$ in dried CH_2Cl_2 for 20 min at 0 °C under N_2. The excess $AlCl_3$ was filtered out with glass wool. The acylating reagent was added by means of a dropping funnel over a period of about 1 h to a solution of biferrocene in dried CH_2Cl_2 at −78 °C. The reaction mixture was stirred for 6 h at −78 °C. The resulting mixture was separated after the reduction of ferrocenium ion with aqueous $Na_2S_2O_3$. The organic layer was washed with saturated aqueous $NaHCO_3$ and water, and it was then dried over $MgSO_4$. The solvent was removed under reduced pressure. The red residue was chromatographed.

The physical properties of **3a** are as follows: ^{1}H NMR (500 MHz, $CDCl_3$) δ 0.93 (t, 3H, $-CH_3$), 1.32 (m, 4H, $-CH_2-$), 1.56 (m, 2H, $-CH_2-$), 2.46 (t, 2H, $-CH_2-$), 3.97 (s, 5H, Cp), 4.21 (t, 4H, Cp), 4.30 (t, 2H, Cp), 4.35 (t, 4H, Cp), 4.58 (t, 2H, Cp); mp 86−88 °C; M^+ at m/z 454. Anal. calcd for $C_{25}H_{26}Fe_2O$: C, 66.11, H, 5.77. Found: C, 66.03, H, 5.80. For **3b**: ^{1}H NMR (500 MHz, $CDCl_3$) δ 1.70 (m, 2H, $-CH_2-$), 1.87 (m, 2H, $-CH_2-$), 2.44 (t, 2H, $-CH_2-$), 3.42 (t, 2H, $-CH_2-$), 3.98 (s, 5H, Cp), 4.22 (t, 4H, Cp), 4.33 (t, 2H, Cp), 4.36 (t, 4H, Cp), 4.59 (t, 2H, Cp); mp 80.0−80.5 °C; M^+ at m/z 532, 534. Anal. calcd for $C_{25}H_{25}BrFe_2O$: C, 56.29, H, 4.69. Found: C, 56.58, H, 4.85. For **3c**: ^{1}H NMR (500 MHz, $CDCl_3$) δ 0.93 (t, 3H, $-CH_3$), 1.33 (m, 2H, $-CH_2-$), 1.57 (m, 2H, $-CH_2-$), 1.71 (m, 2H, $-CH_2-$), 1.87 (m, 2H, $-CH_2-$), 2.44 (t, 4H, $-CH_2-$), 3.42 (t, 2H, $-CH_2-$), 4.26 (m, 4H, Cp), 4.30 (t, 2H, Cp), 4.32 (t, 2H, Cp), 4.35 (m, 4H, Cp), 4.57 (m, 4H, Cp); mp 104−105 °C; M^+ at m/z 616, 618. Anal. Calcd for $C_{30}H_{33}BrFe_2O_2$: C, 58.39, H, 5.39. Found: C, 58.08, H, 5.54. For **3d**: ^{1}H NMR (500 MHz, $CDCl_3$) δ 1.71 (m, 4H, $-CH_2-$), 1.87 (m, 4H, $-CH_2-$), 2.44 (m, 4H, $-CH_2-$), 3.42 (t, 4H, $-CH_2-$), 4.27 (t, 4H, Cp), 4.32 (t, 4H, Cp), 4.35 (t, 4H, Cp), 4.58 (t, 4H, Cp); mp 106−107 °C; M^+ at m/z 694, 696, 698. Anal. Calcd for $C_{30}H_{32}Br_2Fe_2O_2$: C, 51.76, H, 4.63. Found: C, 51.38, H, 4.60.

(29) Dong, T.-Y.; Lai, L. L. *J. Organomet. Chem.* **1996**, *509*, 131.

General Reduction of Acylbiferrocene. The reduction reaction was carried out by carefully adding, with stirring, small portions of $AlCl_3$ to a mixture of acylbiferrocene and $LiAlH_4$ in dried ether. After 40 min, an excess of H_2O was added to it, and the ether layer was separated. The ether layer was washed with water and dried over $MgSO_4$. After the evaporation of the solvent the crude product was chromatographed. All new compounds gave satisfactory spectroscopic and analytical data. Selected physical data for neutral **2a**: mp 81.5−82 °C; M^+ m/z 440; ^{1}H NMR (500 MHz, $CDCl_3$) δ 0.88 (t, 3H, CH_3), 1.21 (m, 2H, CH_2), 1.27 (m, 2H, CH_2), 1.39 (m, 2H, CH_2), 2.11 (t, 2H, CH_2), 3.85 (t, 2H, Cp), 3.89 (t, 2H, Cp), 3.99 (s, 5H, Cp), 4.12 (t, 2H, Cp), 4.17 (t, 2H, Cp), 4.26 (t, 2H, Cp), 4.35 (t, 2H, Cp). For neutral **2b**: mp 94.5−95.5 °C; M^+ m/z 518, 520; ^{1}H NMR (500 MHz, $CDCl_3$) δ 1.38 (m, 4H, CH_2), 1.82 (t, 2H, CH_2), 2.11 (t, 2H, CH_2), 3.38 (t, 2H, CH_2), 3.84 (t, 2H, Cp), 3.89 (t, 2H, Cp), 3.98 (s, 5H, Cp), 4.12 (t, 2H, Cp), 4.18 (t, 2H, Cp), 4.26 (t, 2H, Cp), 4.34 (t, 2H, Cp). For neutral **2c**: mp 34−36 °C; M^+ m/z 588, 590; ^{1}H NMR (500 MHz, $CDCl_3$) δ 0.87 (t, 3H, CH_3), 1.26 (m, 4H, CH_2), 1.38 (M, 4H, CH_2), 1.81 (t, 4H, CH_2), 2.09 (t, 4H, CH_2), 3.38 (t, 2H, CH_2), 3.83 (s, 4H, Cp), 3.88 (t, 4H, Cp), 4.12 (s, 4H, Cp), 4.24 (s, 4H, Cp). For neutral **2d**: mp 68.5−69.5 °C; M^+ m/z 666, 668, 670; ^{1}H NMR (500 MHz, $CDCl_3$) δ 1.37 (m, 8H, CH_2), 1.81 (t, 4H, CH_2), 2.09 (t, 4H, CH_2), 3.38 (t, 4H, CH_2), 3.83 (t, 4H, Cp), 3.89 (t, 4H, Cp), 4.13 (t, 4H, Cp), 4.24 (t, 4H, Cp). For neutral **2e**: mp 59.5−61 °C; M^+ m/z 695, 697, 699; ^{1}H NMR (500 MHz, $CDCl_3$) δ 1.24 (m, 4H, CH_2), 1.38 (m, 8H, CH_2), 1.83 (m, 4H, CH_2), 2.08 (t, 4H, CH_2), 3.40 (t, 4H, CH_2), 3.83 (t, 4H, Cp), 3.88 (t, 4H, Cp), 4.12 (t, 4H, Cp), 4.24 (t, 4H, Cp).

Mixed-Valence Compounds. Compounds were prepared according to the simple procedure previously reported for biferrocenium triiodide.[2−4] Microcrystalline samples were prepared by adding a benzene/hexane (1:1) solution containing a stoichiometric amount of I_2 to a benzene/hexane (1:1) solution of the corresponding neutral biferrocene at 0 °C. A crystalline sample can be prepared by slowly diffusing hexane into a CH_2Cl_2 solution containing the corresponding biferrocenium salt. Microanalyses of the two different preparations were identical within experimental error. Anal. Calcd for **1e** ($C_{30}H_{38}Fe_2I_3$): C, 40.44; H, 4.30. Found: C, 40.44; H, 4.34. Anal. Calcd for **2a** ($C_{25}H_{28}Fe_2I_3$): C, 36.58; H, 3.44. Found: C, 36.63; H, 3.47. Anal. Calcd for **2b** ($C_{25}H_{27}BrFe_2I_3$): C, 33.37; H, 3.02. Found: C, 33.44; H, 3.10. Anal. Calcd for **2c** ($C_{30}H_{37}BrFe_2I_3$): C, 37.15; H, 3.84. Found: C, 36.84; H, 3.88. Anal. Calcd for **2d** ($C_{30}H_{36}Br_2Fe_2I_3$): C, 34.36; H, 3.46. Found: C, 34.27; H, 3.44. Anal. Calcd for **2e** ($C_{32}H_{40}Br_2Fe_2I_3$): C, 35.69; H, 3.74. Found: C, 35.78; H, 3.52.

Physical Methods. The ^{57}Fe Mössbauer spectra were run on a constant-acceleration instrument, which has been previously described.[23] Velocity calibration was made using a 99.99% pure 10 μm iron foil. Typical line widths for all three pairs of iron foil lines fell in the range 0.24−0.27 mm s^{-1}. Isomer shifts are reported relative to iron foil at 300 K but are uncorrected for temperature-dependent Doppler effects. It should be noted that the isomer shifts illustrated in the figures are plotted as experimentally obtained. Tabulated data are provided. ^{1}H NMR spectra were run on a Varian UNITY-INOVA-500 spectrometer. Mass spectra were obtained with a VG-BLOTECH-QUATTRO 5022 system. Electrochemical measurements were carried out with a BAS 100W system. Cyclic voltammetry was performed with a stationary Pt working electrode. These experiments were carried out with a 1×10^{-3} M solution of biferrocene in CH_2Cl_2/CH_3CN (1:1) containing 0.1 M of $(n\text{-}C_4H_9)_4NPF_6$ as supporting electrolyte. The potentials quoted in this work are relative to a Ag/AgCl electrode at 25 °C.

The single-crystal X-ray determinations of compounds **2c** and **2d** were carried out on an Enraf Nonius CAD4 diffractometer and on a Siemens CCD diffractometer for **1e**, **2b**, and **2e**. Absorption corrections were made with empirical φ rota-

tion. The structures were solved from heavy-atom electron density maps and refined by full-matrix least-squares analysis. All non-hydrogen atoms were refined anisotropically. During the final cycles of refinement fixed hydrogen contributions with C−H bond lengths fixed at 0.98 Å were applied. Complete tables of bond distances and angles and thermal parameters of these compounds are given in the Supporting Information.

Structure Determination of 1e. A dark green crystal (0.52 × 0.10 × 0.06 mm) was grown when a layer of hexane was allowed to slowly diffuse into a CH_2Cl_2 solution of **1e**. Data were collected with θ in the range 0.87−27.50°. Of the 18 973 reflections collected, there were 6929 with $F_o^2 > 2.0\sigma(F_o^2)$.

Structure Determination of 2b. A dark green crystal (0.12 × 0.12 × 0.02 mm) was grown when a layer of hexane was allowed to slowly diffuse into a CH_2Cl_2 solution of **2b**. Data were collected with θ in the range 1.80−27.50°. Of the 14 087 reflections collected, there were 3240 with $F_o^2 > 2.0\sigma(F_o^2)$.

Structure Determination of 2c. A dark green crystal (0.60 × 0.20 × 0.10 mm) was grown when a layer of hexane was allowed to slowly diffuse into a CH_2Cl_2 solution of **2c**. Data were collected with θ in the range 1.83−24.97°. Of the 5656 reflections collected, there were 5656 with $F_o^2 > 2.0\sigma(F_o^2)$.

Structure Determination of 2d. A dark green crystal (0.60 × 0.05 × 0.01 mm) was grown when a layer of hexane was allowed to slowly diffuse into a CH_2Cl_2 solution of **2d**. Data were collected with θ in the range 2.31−27.50°. Of the 3755 reflections collected, there were 3755 with $F_o^2 > 2.0\sigma(F_o^2)$.

Structure Determination of 2e. A dark green crystal (0.35 × 0.20 × 0.05 mm) was grown when a layer of hexane was allowed to slowly diffuse into a CH_2Cl_2 solution of **2e**. Data were collected with θ in the range 2.13−27.50°. Of the 19 204 reflections collected, there were 7657 with $F_o^2 > 2.0\sigma(F_o^2)$.

Acknowledgments are made to the National Science Council (NSC89-2113-M-110-019) and the Department of Chemistry at National Sun Yat-Sen University, Taiwan.

Supporting Information Available: Complete tables of positional parameters, bond distances and angles, and thermal parameters for **1e**, **2b**, **2c**, **2d**, and **2e**. This material is available free of charge via the Internet at http://pubs.acs.org.

OM0203476